Projection finite volume method for shallow water flows

Fayssal Benkhaldoun [a], Saida Sari [a,*], Mohammed Seaid [b]

[a] *LAGA, Université Paris* 13, 99 *Av J.B. Clement,* 93430 *Villetaneuse, France*

[b] *School of Engineering and Computing Sciences, University of Durham, South Road, DH1 3LE, UK*

Abstract

A simple and accurate projection finite volume method is developed for solving shallow water equations in two space dimensions. The proposed approach belongs to the class of fractional-step procedures where the numerical fluxes are reconstructed using the method of characteristics, while an Eulerian method is used to discretize the conservation equations in a finite volume framework. The method is conservative and it combines advantages of the method of characteristics to accurately solve the shallow water flows with an Eulerian finite volume method to discretize the equations. Numerical results are presented for several applications in rotating shallow water problems. The aim of such a method compared to the conventional finite volume methods is to solve shallow water equations efficiently and with an appropriate level of accuracy.

Key words: Finite volume discretization, Projection method, Method of characteristics, Shallow water equations, Rotating flows

1 Introduction

Modeling shallow water flows with Coriolis forces is useful to study hydraulic engineering problems involving rotating flows in meteorology and climate research, and other applications in coastal hydrodynamics. The mathematical governing equations are commonly achieved by vertical integration of the Navier-Stokes equations along with the assumptions of a hydrostatic pressure and a vertically uniform horizontal velocity profile. Many numerical methods

* Corresponding author.
Email address: sari@math.univ-paris13.fr (Saida Sari).

are available in the literature to solve the shallow water equations. The most popular techniques are based on the well-known Roe scheme [11] originally designed for hyperbolic systems of conservation laws without accounting for source terms. The authors in [1] have also developed exact solutions for the Riemann problem at the interface with a sudden variation of the topography in shallow water equations. The main idea in their approach was to define the bottom level such that a sudden variation in the topography occurs at the interface of two cells. An approach based on a local hydrostatic reconstruction has been proposed in [2] for open channel flows with topography. The extension of ENO and WENO schemes to shallow water equations has been studied in [15]. Unfortunately, most ENO and WENO schemes that solves real flows correctly are still very computationally expensive. On the other hand, numerical methods based on kinetic reconstructions have been studied in [13] among others, but the complexity of these methods is relevant.

In [4], the authors proposed a simple and accurate method for solving the one-dimensional shallow water equations on non-flat beds. This method incorporates the techniques from method of characteristics into the reconstruction of numerical fluxes. The performance of the proposed method has been demonstrated for several test examples on shallow water equations in one space dimension. In this paper we extend this method to two-dimensional shallow water equations with Coriolis forces. Our main goal is to present a class of numerical methods that are simple, easy to implement, and accurately solves the shallow water equations without relying on a Riemann solver. This goal is reached by a projection of the shallow water system in the local coordinates and a method of characteristics is used. In the first step, the conservation equations are integrated over an Eulerian control volume. We term this step by corrector stage applied to the conservation equations. In the second step, the shallow water equations are projected in a non-conservative form and integrated along the characteristics defined by the water velocity. This step is called predictor stage and used to calculate the numerical fluxes required in the corrector stage. Our method can be treated as a conservative modified method of characteristics for shallow water equations or as a Riemann solver-free finite volume method for shallow water equations. The discretization of flux gradients and source terms are well-balanced and the method satisfies the exact C-property. The proposed scheme has the ability to handle calculations of slowly varying flows as well as rapidly varying flows over continuous and discontinuities bottom beds. These features are demonstrated using several benchmark problems for two-dimensional shallow water flows. Results presented in this paper show high resolution of the proposed finite volume characteristics method and confirm its capability to provide accurate and efficient simulations for shallow water flows including Coriolis forces.

This paper is organized as follows. The rotating shallow water equations and their projection finite volume discretization are presented in section 2. In sec-

tion 3, the method of characteristics is formulated for the reconstruction of the numerical fluxes. This section includes also the discretization of the source terms. Section 4 is devoted to numerical results for several test examples for rotating shallow water equations. Our new approach is shown to enjoy the expected accuracy as well as the robustness. Section 5 contains concluding remarks.

2 Projection method for shallow water equations

The two-dimensional shallow water equations represent mass and momentum conservation and have been widely used to model water flows under the influence of gravity. In a conservative form these equations are formulated as

$$\begin{aligned}
&\frac{\partial h}{\partial t} + \frac{\partial (hu)}{\partial x} + \frac{\partial (hv)}{\partial y} = 0, \\
&\frac{\partial (hu)}{\partial t} + \frac{\partial}{\partial x}\left(hu^2 + \frac{1}{2}gh^2\right) + \frac{\partial}{\partial y}\left(huv\right) = -gh\frac{\partial Z}{\partial x} + f_c hv, \\
&\frac{\partial (hv)}{\partial t} + \frac{\partial}{\partial x}\left(huv\right) + \frac{\partial}{\partial y}\left(hv^2 + \frac{1}{2}gh^2\right) = -gh\frac{\partial Z}{\partial y} - f_c hu,
\end{aligned} \tag{1}$$

where g is the gravitational acceleration, f_c is the Coriolis parameter defined by $f_c = 2\omega \sin\phi$, with ω denoting the angular velocity of the earth and ϕ is the geographic latitude, $h(t,x,y)$ is the water depth, $u(t,x,y)$ and $v(t,x,y)$ are the depth-averaged velocities in the x- and y-direction, respectively. In the present work, we neglect diffusion by viscous or turbulent effects, the wind effects and friction forces in the momentum equation. It is well known that the system (1) is strictly hyperbolic with real and distinct eigenvalues. For simplicity in presentation we rewrite the equations (1) in a conservative form as

$$\frac{\partial \mathbf{W}}{\partial t} + \frac{\partial \mathbf{F}(\mathbf{W})}{\partial x} + \frac{\partial \mathbf{G}(\mathbf{W})}{\partial y} = \mathbf{Q}(\mathbf{W}) + \mathbf{R}(\mathbf{W}), \tag{2}$$

where

$$\mathbf{W} = \begin{pmatrix} h \\ hu \\ hv \end{pmatrix}, \quad \mathbf{F}(\mathbf{W}) = \begin{pmatrix} hu \\ hu^2 + \frac{1}{2}gh^2 \\ huv \end{pmatrix}, \quad \mathbf{G}(\mathbf{W}) = \begin{pmatrix} hv \\ huv \\ hv^2 + \frac{1}{2}gh^2 \end{pmatrix},$$

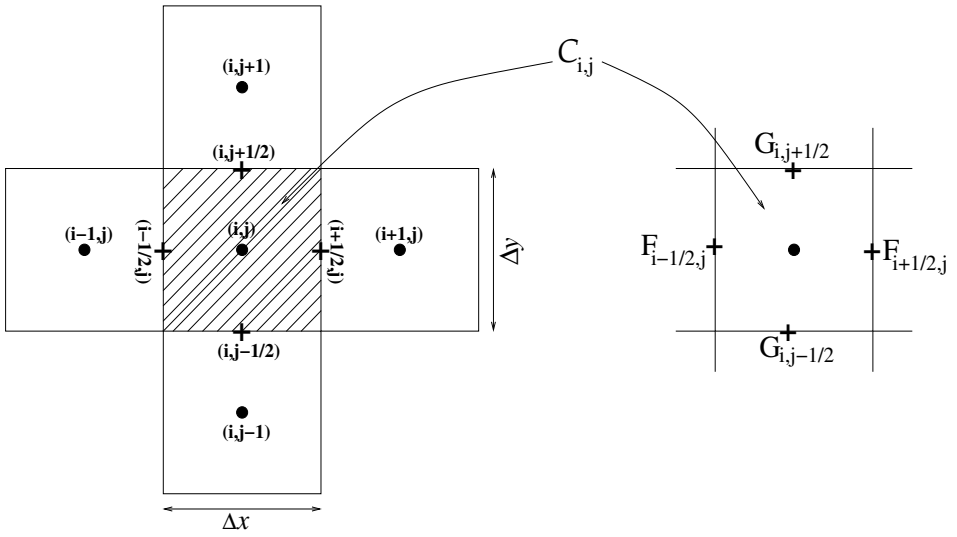

Fig. 1. An illustration of control volumes $\mathcal{C}_{i,j}$ used in the proposed method.

$$\mathbf{Q}(\mathbf{W}) = \begin{pmatrix} 0 \\ -gh\dfrac{\partial Z}{\partial x} \\ -gh\dfrac{\partial Z}{\partial y} \end{pmatrix}, \quad \mathbf{R}(\mathbf{W}) = \begin{pmatrix} 0 \\ f_c hv \\ -f_c hu \end{pmatrix},$$

Note that the equations (2) has to be solved in a bounded spatial domain Ω with smooth boundary Γ, equipped with given boundary and initial conditions. In practice, these conditions are problem dependent and their discussion is postponed for section 3 where numerical examples are discussed.

Let us cover the spatial domain Ω with cells $\mathcal{C}_{ij} = [x_{i-\frac{1}{2}}, x_{i+\frac{1}{2}}] \times [y_{j-\frac{1}{2}}, y_{j+\frac{1}{2}}]$ shown in Figure 1. The cells, $\mathcal{C}_{ij}$, are centered at $(x_i = i\Delta x, y_j = j\Delta y)$ with uniform sizes Δx and Δy for simplicity in the presentation only. Integrating (1) over the element $\mathcal{C}_{ij}$, the basic equations of the finite volume method obtained using the divergence theorem are given by

$$\frac{\partial}{\partial t}\int_{\mathcal{C}_{i,j}} h\, dV + \oint_{\mathcal{S}_{i,j}} (hun_x + hvn_y)\; d\sigma = 0,$$

$$\frac{\partial}{\partial t}\int_{\mathcal{C}_{i,j}} hu\, dV + \oint_{\mathcal{S}_{i,j}} \left(\left(hu^2 + \frac{1}{2}gh^2\right)n_x + huvn_y\right) d\sigma = -gh\oint_{\mathcal{S}_{i,j}} Zn_x\, d\sigma + \int_{\mathcal{C}_{i,j}} f_c hv\, dV,$$

$$\frac{\partial}{\partial t}\int_{\mathcal{C}_{i,j}} hv\, dV + \oint_{\mathcal{S}_{i,j}} \left(huvn_x + \left(hv^2 + \frac{1}{2}gh^2\right)n_y\right) d\sigma = -gh\oint_{S_i} Zn_y\, d\sigma - \int_{\mathcal{C}_{i,j}} f_c hu\, dV,$$

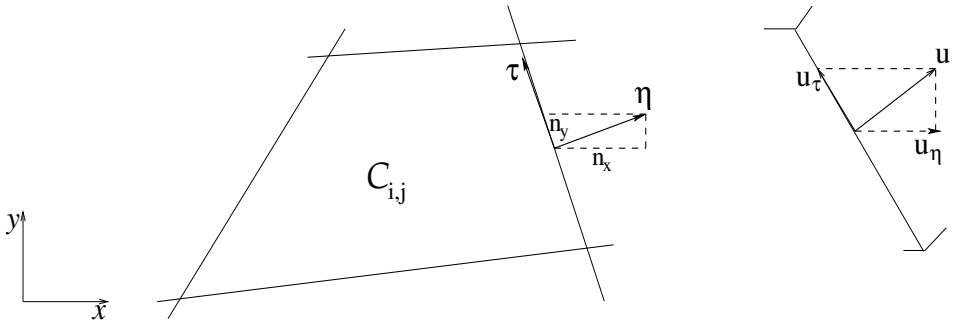

Fig. 2. Illustration of the projected velocities on the control volume $\mathcal{C}_{i,j}$.

where $\eta = (n_x, n_y)^T$ denotes the unit outward normal to the surface $\mathcal{S}_{i,j}$ of the element $\mathcal{C}_{ij}$. Using the local cell outward normal η and tangential $\tau = \eta^{\perp}$ depicted in Figure 2, the above equations can be projected as

$$\frac{\partial}{\partial t}\int_{\mathcal{C}_{i,j}} h\, dV + \oint_{\mathcal{S}_{i,j}} hu_\eta\, d\sigma = 0, \tag{3a}$$

$$\frac{\partial}{\partial t}\int_{\mathcal{C}_{i,j}} hu\, dV + \oint_{\mathcal{S}_{i,j}} \left(huu_\eta + \frac{1}{2}gh^2 n_x\right)\, d\sigma = -gh\oint_{S_i} Z n_x\, d\sigma + \int_{\mathcal{C}_{i,j}} f_c hv\, dV, \tag{3b}$$

$$\frac{\partial}{\partial t}\int_{\mathcal{C}_{i,j}} hv\, dV + \oint_{\mathcal{S}_{i,j}} \left(hvu_\eta + \frac{1}{2}gh^2 n_y\right)\, d\sigma = -gh\oint_{S_i} Z n_y\, d\sigma - \int_{\mathcal{C}_{i,j}} f_c hu\, dV, \tag{3c}$$

where the normal projected velocity $u_\eta = un_x + vn_y$ and the tangential projected velocity $u_\tau = vn_x - un_y$. In order to simplify the system (3), we first sum the equation (3b) multiplied by n_x to the equation (3c) multiplied by n_y, then we subtract the equation (3b) multiplied by n_y from the equation (3c) multiplied by n_x. The outcome of these operations is

$$\begin{aligned}
\frac{\partial}{\partial t}\int_{\mathcal{C}_{i,j}} h\, dV + \oint_{\mathcal{S}_{i,j}} hu_\eta\, d\sigma &= 0,\\
\frac{\partial}{\partial t}\int_{\mathcal{C}_{i,j}} hu_\eta\, dV + \oint_{\mathcal{S}_{i,j}} \left(hu_\eta u_\eta + \frac{1}{2}gh^2\right)\, d\sigma &= -gh\oint_{S_i} Z\, d\sigma + \int_{\mathcal{C}_{i,j}} f_c hu_\tau\, dV,\\
\frac{\partial}{\partial t}\int_{\mathcal{C}_{i,j}} hu_\tau\, dV + \oint_{\mathcal{S}_{i,j}} hu_\tau u_\eta\, d\sigma &= -\int_{\mathcal{C}_{i,j}} f_c hu_\eta\, dV,
\end{aligned}$$

which can be rewritten in a differential form as

$$
\begin{aligned}
\frac{\partial h}{\partial t} + \frac{\partial \left(h u_\eta\right)}{\partial \eta} &= 0, \\
\frac{\partial \left(h u_\eta\right)}{\partial t} + \frac{\partial}{\partial \eta}\left(h u_\eta^2 + \frac{1}{2} g h^2\right) &= -g h \frac{\partial Z}{\partial \eta} - f_c h u_\tau, \\
\frac{\partial \left(h u_\tau\right)}{\partial t} + \frac{\partial}{\partial \eta}\left(h u_\eta u_\tau\right) &= f_c h u_\eta.
\end{aligned} \tag{4}
$$

The system (4) can also be reformulated in a non-conservative form as

$$
\begin{aligned}
\frac{Dh}{Dt} + h \frac{\partial u_\eta}{\partial \eta} &= 0, \\
\frac{Du_\eta}{Dt} + g \frac{\partial h}{\partial \eta} &= -g \frac{\partial Z}{\partial \eta} - f_c u_\tau, \\
\frac{Du_\tau}{Dt} + h \frac{\partial u_\tau}{\partial \eta} &= f_c u_\eta,
\end{aligned} \tag{5}
$$

where $\frac{D}{Dt} = \frac{\partial}{\partial t} + u_\eta \frac{\partial}{\partial \eta}$ is the total material derivative. The system (5) can also be rearranged in a compact vector form as

$$
\frac{D\mathbf{U}}{Dt} = \mathbf{S}(\mathbf{U}), \tag{6}
$$

where

$$
\mathbf{U} = \begin{pmatrix} h \\ u_\eta \\ u_\tau \end{pmatrix}, \quad \mathbf{S}(\mathbf{U}) = \begin{pmatrix} -h \dfrac{\partial u_\eta}{\partial \eta} \\ -g \dfrac{\partial \left(h + Z\right)}{\partial \eta} - f_c u_\tau \\ -h \dfrac{\partial u_\tau}{\partial \eta} + f_c u_\eta \end{pmatrix}.
$$

Note that using the projection method on the local coordinates the two-dimensional shallow water equations (1) in the control volume $\mathcal{C}_{i,j}$ reduce to the one-dimensional system (6) on each surface $\mathcal{S}_{i,j}$ of this control volume. In the proposed method the system (6) is used only to reconstruct the numerical fluxes while the finite volume method is applied directly to the conservative system (1). Similar projection techniques have also been used in [12,5] among others.

3 Finite volume characteristics method

In this section we formulate the finite volume characteristics method for the numerical solution of the shallow water equations (1). The method consists of two steps and can be interpreted as a predictor-corrector approach. The first

step deals with the finite volume discretization of the equations whereas in the second step, reconstruction of the numerical fluxes is discussed.

3.1 Finite volume discretization

For the space discretization of the equations (2), we use the notations

$$\mathbf{W}_{i\pm\frac{1}{2},j}(t) = \mathbf{W}(t, x_{i\pm\frac{1}{2}}, y_j), \qquad \mathbf{W}_{i,j\pm\frac{1}{2}}(t) = \mathbf{W}(t, x_i, y_{j\pm\frac{1}{2}}),$$

$$\text{and} \qquad \mathbf{W}_{i,j}(t) = \frac{1}{\Delta x}\frac{1}{\Delta y}\int_{x_{i-\frac{1}{2}}}^{x_{i+\frac{1}{2}}}\int_{y_{j-\frac{1}{2}}}^{y_{i+\frac{1}{2}}} \mathbf{W}(t,x,y)dydx,$$

to denote the point-values and the approximate cell-average of the variable $\mathbf{W}$ at the gridpoint $(t, x_{i\pm\frac{1}{2}}, y_j)$, $(t, x_i, y_{j\pm\frac{1}{2}})$, and (t, x_i, y_j), respectively. Integrating the equation (2) with respect to space over the control volume $\mathcal{C}_{i,j}$ shown in Figure 1, we obtain the following semi-discrete equation

$$\frac{d\mathbf{W}_{i,j}}{dt} + \frac{\mathbf{F}_{i+1/2,j} - \mathbf{F}_{i-1/2,j}}{\Delta x} + \frac{\mathbf{G}_{i,j+1/2} - \mathbf{G}_{i,j-1/2}}{\Delta y} = \mathbf{Q}_{i,j} + \mathbf{R}_{i,j}, \qquad (7)$$

where $\mathbf{F}_{i\pm1/2,j} = \mathbf{F}(\mathbf{W}_{i\pm1/2,j})$ and $\mathbf{G}_{i,j\pm1/2} = \mathbf{G}(\mathbf{W}_{i,j\pm1/2})$ are the numerical fluxes at the cell interfaces $x = x_{i\pm1/2}$ and $y = y_{i\pm1/2}$, respectively. In (7), $\mathbf{Q}_{i,j}$ and $\mathbf{R}_{i,j}$ are consistent discretizations of the source terms $\mathbf{Q}$ and $\mathbf{R}$ in (2). The spatial discretization of equation (7) is complete when a time integration is performed and a numerical construction of the fluxes $\mathbf{F}_{i\pm1/2,j}$ and $\mathbf{G}_{i,j\pm1/2}$ is chosen. In general, this construction requires a solution of Riemann problems at the interfaces $x_{i\pm1/2}$ and $y_{i\pm1/2}$, see for example [11,12,5]. From a computational viewpoint, this procedure is very demanding and may restrict the application of the method to shallow water equations for which Riemann solutions are available.

To integrate the equations (7) in time we divide the time interval into N subintervals $[t_n, t_{n+1}]$ with length $\Delta t = t_{n+1} - t_n$ for $n = 0, 1, \ldots, N$. We use the notation w^n to denote the value of a generic function w at time t_n. We may consider a first-order two-step time stepping scheme, in which the fully-discrete formulation of the system (2) is given by

$$\begin{aligned}
\widetilde{\mathbf{W}}_{i,j} &= \mathbf{W}^n_{i,j} + \Delta t \mathbf{R}^n_{i,j}, \\
\mathbf{W}^{n+1}_{i,j} &= \widetilde{\mathbf{W}}_{i,j} - \frac{\Delta t}{\Delta x}\left(\widetilde{\mathbf{F}}^n_{i+1/2,j} - \widetilde{\mathbf{F}}^n_{i-1/2,j}\right) - \\
&\quad \frac{\Delta t}{\Delta y}\left(\widetilde{\mathbf{G}}^n_{i,j+1/2} - \widetilde{\mathbf{G}}^n_{i,j-1/2}\right) + \Delta t \widetilde{\mathbf{Q}}^n_{i,j},
\end{aligned} \qquad (8)$$

where $\widetilde{\mathbf{F}}^n_{i\pm1/2,j} = \mathbf{F}(\widetilde{\mathbf{W}}^n_{i\pm1/2,j})$ and $\widetilde{\mathbf{G}}^n_{i,j\pm1/2} = \mathbf{G}(\widetilde{\mathbf{W}}^n_{i,j\pm1/2})$. Note that other

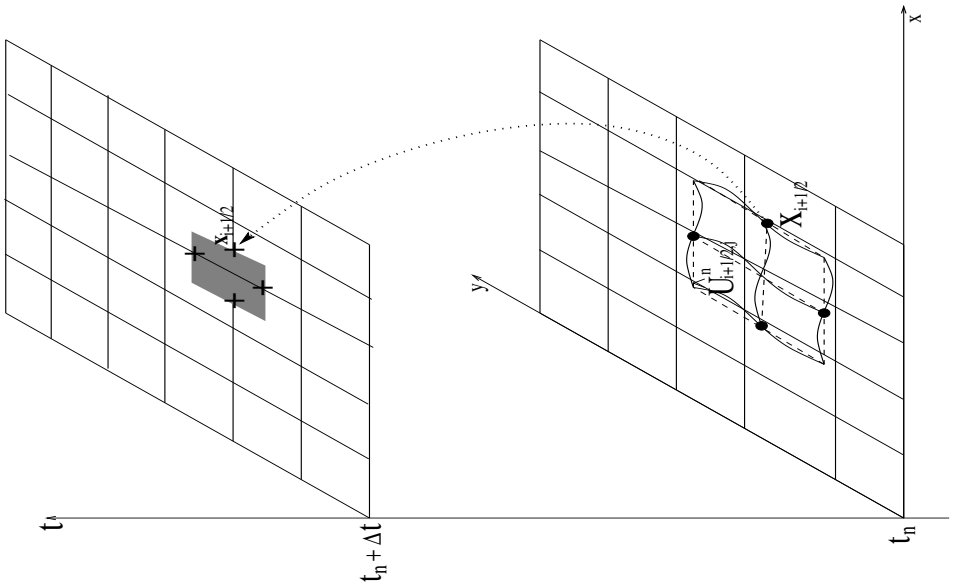

Fig. 3. Sketch of the method of characteristics: A water particle at gridpoint $x_{i+1/2}$ is traced back in time to $X_{i+1/2}$ where the intermediate solution $\hat{U}^n_{i+1/2,j}$ is interpolated.

high-order time stepping methods can also be applied without major conceptual modifications. It should also be noted that using the splitting (8) the Coriolis forces are supposed to be updated separately in the first step of the splitting whereas, the second step deals with the remaining source terms.

3.2 Method of characteristics

In the present study, we reconstruct the numerical fluxes $\mathbf{F}_{i\pm1/2,j}$ and $\mathbf{G}_{i,j\pm1/2}$ using the method of characteristics. The fundamental idea of this method is to impose a regular grid at the new time level and to backtrack the flow trajectories to the previous time level, see for example [10,14]. At the old time level, the quantities that are needed are evaluated by interpolation from their known values on a regular grid. Hence, the characteristic curves associated with the equations (6) are solutions of the initial-value problems

$$\begin{aligned} \frac{dX_{i+1/2}(s)}{ds} &= u_\eta\Big(s, X_{i+1/2}(s)\Big), \qquad s \in [t_n, t_n + \Delta t], \\ X_{i+1/2}(t_n + \Delta t) &= x_{i+1/2}, \end{aligned} \tag{9}$$

with a similar system of the characteristic curves $Y_{j+1/2}(s)$ in the y-direction. Note that $X_{i+1/2}(s)$ (respectively $Y_{j+1/2}(s)$) is the departure point at time s of a particle that will arrive at the gridpoint $x_{i+1/2}$ (respectively $y_{j+1/2}(s)$) in time $t_n + \Delta t$, compare Figure 3. The method of characteristics does not follow

the flow particles forward in time, as the Lagrangian schemes do, instead it traces backwards the position at time t_n of particles that will reach the points of a fixed mesh at time $t_n + \Delta t$. By doing so, the method avoids the grid distortion difficulties that the conventional Lagrangian schemes have. Hence, the solution of (9) can be expressed in an integral form as

$$X_{i+1/2,j}(t_n) = x_{i+1/2,j} - \int_{t_n}^{t_n+\Delta t} u_\eta \left(s, X_{i+1/2,j}(s)\right) ds. \tag{10}$$

In our simulations we used a first-order Euler method to approximate the integral in (10), however other high-order Runge-Kutta methods are also possible. In general $X_{i+1/2,j}(t_n)$ (respectively $Y_{j+1/2}(t_n)$) will not coincide with the spatial position of a gridpoint. Thus, once the characteristic curves $X_{i+1/2,j}(t_n)$ (respectively $Y_{j+1/2}(t_n)$) are accurately calculated, the intermediate solutions $W^n_{i+1/2,j}$ and $W^n_{i,j+1/2}$ of a generic function W are reconstructed using

$$W^n_{i+1/2,j} = \widehat{W}^n_{i+1/2,j}, \qquad W^n_{i,j+1/2} = \widehat{W}^n_{i,j+1/2}, \tag{11}$$

where $\widehat{W}^n_{i+1/2,j} = W\left(t_n, X_{i+1/2}(t_n), y_j\right)$ and $\widehat{W}^n_{i,j+1/2} = W\left(t_n, x_i, Y_{j+1/2}(t_n)\right)$ are the solutions at the characteristic feet computed by interpolation from the gridpoints of the control volume where the departure points reside, see Figure 3 for an illustration. For instance, a Lagrange-based interpolation polynomials can be formulated as

$$\begin{aligned} \widehat{W}^n_{i+1/2,j} &= \sum_{k,l} \mathcal{L}_{k,l}(X_{i+1/2}, y_j) W^n_{k,l}, \\ \widehat{W}^n_{i,j+1/2} &= \sum_{k,l} \mathcal{L}_{k,l}(x_i, Y_{j+1/2}) W^n_{k,l}, \end{aligned} \tag{12}$$

with $\mathcal{L}_{k,l}$ are the Lagrange basis polynomials given by

$$\mathcal{L}_{k,l}(x,y) = \prod_{\substack{p=0 \\ p\neq k}} \prod_{\substack{q=0 \\ q\neq l}} \frac{x - x_p}{x_k - x_p} \frac{y - y_q}{y_l - y_q}.$$

Note that other interpolation procedures such as Spline or Hermite interpolation methods or interpolation techniques based on radial basis functions can also be applied. Assume an accurate approximation of the characteristics curves $X_{i+1/2,j}(t_n)$ is made, the predictor stage in the FVC method applied to the shallow water equations is defined by the solution of the system (6) as

$$\mathbf{U}^n_{i+1/2,j} = \widehat{\mathbf{U}}^n_{i+1/2,j} + \Delta t \mathbf{S}\left(\widehat{\mathbf{U}}^n_{i+1/2,j}\right). \tag{13}$$

Following similar techniques in [4] for the one-dimensional shallow water equations, a difference discretization of the source terms in (13) yields

$$
\begin{aligned}
h^n_{i+1/2,j} &= \widehat{h}^n_{i+1/2,j} - \frac{\Delta t}{\Delta x}\widehat{h}^n_{i+1/2,j}\left((u_\eta)^n_{i+1,j} - (u_\eta)^n_{i,j}\right), \\
(u_\eta)^n_{i+1/2,j} &= (\widehat{u}_\eta)^n_{i+1/2,j} - g\frac{\Delta t}{\Delta x}\Big((h^n+Z)_{i+1,j} - (h^n+Z)_{i,j}\Big) - \\
&\quad \Delta t f_c\,(\widehat{u}_\tau)^n_{i+1/2,j}\,, \\
(u_\tau)^n_{i+1/2,j} &= (\widehat{u}_\tau)^n_{i+1/2,j} - \frac{\Delta t}{\Delta x}\widehat{h}^n_{i+1/2,j}\left((u_\tau)^n_{i+1,j} - (u_\tau)^n_{i,j}\right) + \\
&\quad \Delta t f_c\,(\widehat{u}_\eta)^n_{i+1/2,j}\,,
\end{aligned}
\tag{14}
$$

where

$$
\widehat{h}^n_{i+1/2,j} = h\left(t_n, X_{i+1/2}(t_n), y_j\right), \qquad (\widehat{u}_\eta)^n_{i+1/2,j} = u_\eta\left(t_n, X_{i+1/2}(t_n), y_j\right),
$$

$$
(\widehat{u}_\tau)^n_{i+1/2,j} = u_\tau\left(t_n, X_{i+1/2}(t_n), y_j\right).
$$

The the intermediate states $\mathbf{U}^n_{i,j+1/2}$ in the y-direction can be evaluated in the same manner. Once the projected states are calculated in the predictor stage (14), the states $\mathbf{W}^n_{i\pm1/2,j}$ and $\mathbf{W}^n_{i,j\pm1/2}$ are recovered by using the transformations $v = (u_\tau, u_\eta)\cdot\eta$ and $u = (u_\tau, u_\eta)\cdot\tau$.

In the proposed method, the discretization of the source terms $\mathbf{Q}_{i,j}$ in (7) is carried out such that the discretization of the source terms are well balanced with the discretization of flux gradients using the concept of C-property [6]. Recall that a numerical scheme is said to satisfy the C-property for the equations (1) if the condition

$$
h^n + Z = C = constant, \qquad u^n = v^n = 0, \tag{15}
$$

holds for stationary flows at rest. Therefore, the treatment of source terms $\mathbf{Q}_{i,j}$ in (7) is reconstructed such that the condition (15) is preserved at the discretized level. Following the same steps in our study reported in [4] for the one-dimensional shallow water equations, the discretization of the terms in (7) is carried out as

$$
\begin{aligned}
\left(gh\frac{\partial Z}{\partial x}\right)^n_{i,j} &= g\frac{h^n_{i+1/2,j} + h^n_{i-1/2,j}}{2}\frac{Z^n_{i+1,j} - Z^n_{i-1,j}}{2\Delta x}, \\
\left(gh\frac{\partial Z}{\partial y}\right)^n_{i,j} &= g\frac{h^n_{i,j+1/2} + h^n_{i,j-1/2}}{2}\frac{Z^n_{i,j+1} - Z^n_{i,j-1}}{2\Delta y},
\end{aligned}
\tag{16}
$$

where the averaged solutions are defined by

$$
h^n_{i+1/2,j} = \frac{h^n_{i+1,j} + h^n_{i-1,j}}{2}, \qquad h^n_{i,j+1/2} = \frac{h^n_{i,j+1} + h^n_{i,j-1}}{2}.
$$

The discretization of source terms in (16) is achieved by projecting the original shallow water model into the local system where a dimension by dimension

discretization is used. Details on this approach can be found in [4] and for brevity they are omitted here. It should be stressed that the C-property is obtained by assuming a linear interpolation procedure in the predictor stage of the FVC method. However, a well-balanced discretization of flux gradients and source terms for a quadratic or cubic interpolation procedures can be carried out using similar techniques.

4 Numerical results

In this section we perform numerical tests with our finite volume characteristics method for the two-dimensional shallow water equations. In all our computations a fixed courant number CFL = 0.8 is used while the time step Δt is varied according to the stability condition

$$\Delta t = \mathrm{CFL}\frac{\min\left(\Delta x, \Delta y\right)}{\max\left(|u^n| + \sqrt{gh^n}, |v^n| + \sqrt{gh^n}\right)}.$$

In all results presented in this section the linear interpolation procedure is used in the predictor stage. For comparison reasons, we also compare the results obtained using our Finite Volume Characteristics (FVC) method to those obtained using the well established Roe scheme in [11] and a modified Roe method (SRNH) developed in [12]. The following test examples are selected:

4.1 Accuracy test examples

We first check the accuracy of the proposed FVC method for a shallow water system with know analytical solution [7]. We solve the shallow water equations (1) without Coriolis force in the squared domain $\Omega = [-50, 50] \times [-50, 50]$ with analytical solution for the water depth and the velocity

$$h(t,x,y) = 1 - \frac{a}{4bg}e^{-2b\left(\bar{x}^2+\bar{y}^2\right)}, \quad u(t,x,y) = \frac{1}{2}\cos\alpha + a\bar{y}e^{-b\left(\bar{x}^2+\bar{y}^2\right)}, \quad v(t,x,y) = \frac{1}{2}\sin\alpha - a\bar{x}e^{-b\left(\bar{x}^2+\bar{y}^2\right)}, \tag{17}$$

where $\bar{x} = x + 20 - \frac{t}{2}\cos\alpha$ and $\bar{y} = y + 10 - \frac{t}{2}\sin\alpha$. Initial and boundary condition are set according to the exact solution (17). Here we use the same parameters as in [7] for $g = 1$, $a = 0.04$, $b = 0.02$ and results are displayed at

Table 1
Relative L^1-error and CPU times (in seconds) obtained for the accuracy test example at time $t = 100$ using the Roe, SRNH and FVC methods.

	Roe		SRNH		FVC	
Gridpoints	L^1-error	CPU	L^1-error	CPU	L^1-error	CPU
50×50	3.0626E-04	9.95	2.9673E-04	10.70	2.6409E-04	2.59
100×100	2.6969E-04	81.26	2.6224E-04	87.96	1.9851E-04	12.01
200×200	2.2984E-04	658.75	2.2269E-04	741.40	1.3651E-04	84.37
400×400	1.7808E-04	5533.40	1.6791E-04	5914.53	8.280E-05	738.85

time $t = 100$. We consider the relative L^1-error norm defined as

$$\frac{\sum_{i=1}^{M}\sum_{j=1}^{M}\left|h_{i,j}^{n} - h(t_n, x_i, y_j)\right|\Delta x\Delta y}{\sum_{i=1}^{M}\sum_{j=1}^{M}\left|h(t_n, x_i, y_j)\right|\Delta x\Delta y}, \tag{18}$$

where $h_{i,j}^{n}$ and $h(t_n, x_i, y_j)$ are respectively, the computed and exact water depth at gridpoint (x_i, y_j), whereas M stands for the number of gridpoints in each direction used in the spatial discretization. The obtained results are listed in Table 1 along with their corresponding CPU times. It reveals that increasing the number of gridpoints in the computational domain results in a decay of L^1-error in all methods. A faster decay of the error is observed in the FVC method than in Roe and SRNH methods. A simple inspection of Table 1 also reveals that, for meshes with low number of gridpoints, the measured CPU time is comparable for Roe and SRNH methods. However, for all considered meshes the FVC method is the most efficient. For instance, for a mesh of 400×400 gridpoints, the FVC method is about 7 and 8 faster than the Roe method and SRNH scheme, respectively. Similar results not reported here have been obtained for the relative L^1-error in the velocities u and v. Note that the Roe and SRNH schemes require a solver for the Riemann problem at each time step to reconstruct the numerical fluxes, which is completely avoided in our FVC scheme.

Next we examine the preservation of the C-property for the proposed FVC method. To this end we consider a two-dimensional version of the benchmark problem of a lake at rest flow proposed in [6] to test the conservation property of numerical methods for one-dimensional shallow water equations. Here we solve the two-dimensional shallow water equations (1) in a channel 1000 m long and 10 m wide using the bed data provided in [6]. For this test problem the gravitational force $g = 9.8\ m/s^2$ and the Coriolis force $f_c = 0$. The channel

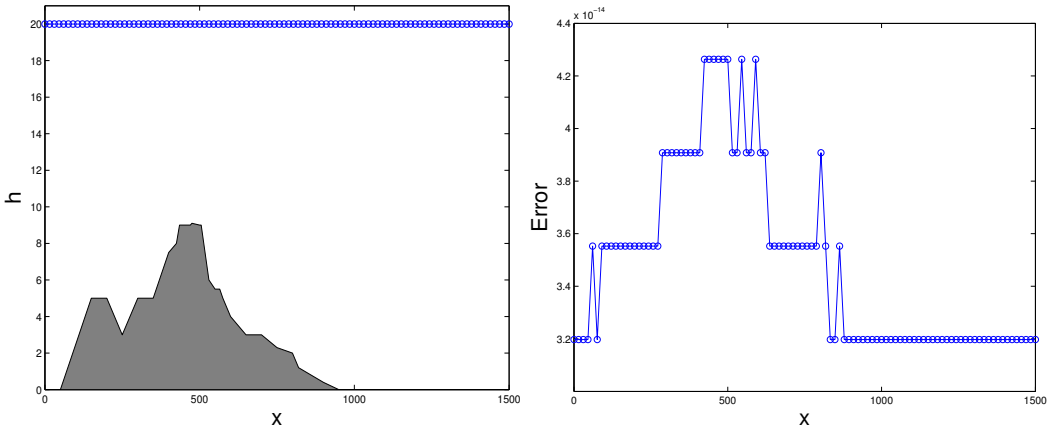

Fig. 4. Cross-sections of the free-surface (left plot) and the error (right plot) for the lake at rest in the middle of the channel $y = 5\ m$ and at time $t = 10800\ s$.

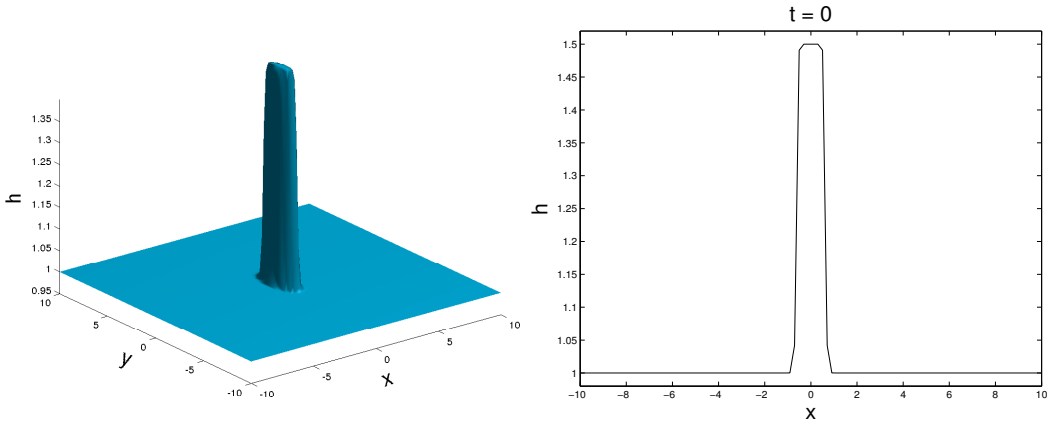

Fig. 5. Initial water depth for the circular dam-break problem on flat bottom (left plot) and its diagonal cross-section at $y = x$ (right plot).

bed is irregular, so this test example is a good illustration of the significance of the source term treatment for practical applications to natural watercourses. It is expected that the water free-surface remains constant and the water velocity should be zero at all times. We run the FVC method using a mesh of 100×100 gridpoints and the obtained results are displayed at time $t = 10800\ s$. In Figure 4 we present the water free-surface along with the bed profile and the surface plot of the absolute error in the water depth defined as $|h + Z - 20|$. For a better insight we also include in this figure the horizontal cross-section at $y = 5\ m$ of the water free-surface and the absolute error along with the channel bed. As can be seen, the water free-surface remains constant during the simulation time and the proposed FVC method preserves the C-property to the machine precision. It should be stressed that the performance of the FVC method is very attractive since the computed solution remains stable and accurate even when coarse meshes are used without requiring complicated techniques to balance the source terms and flux gradients.

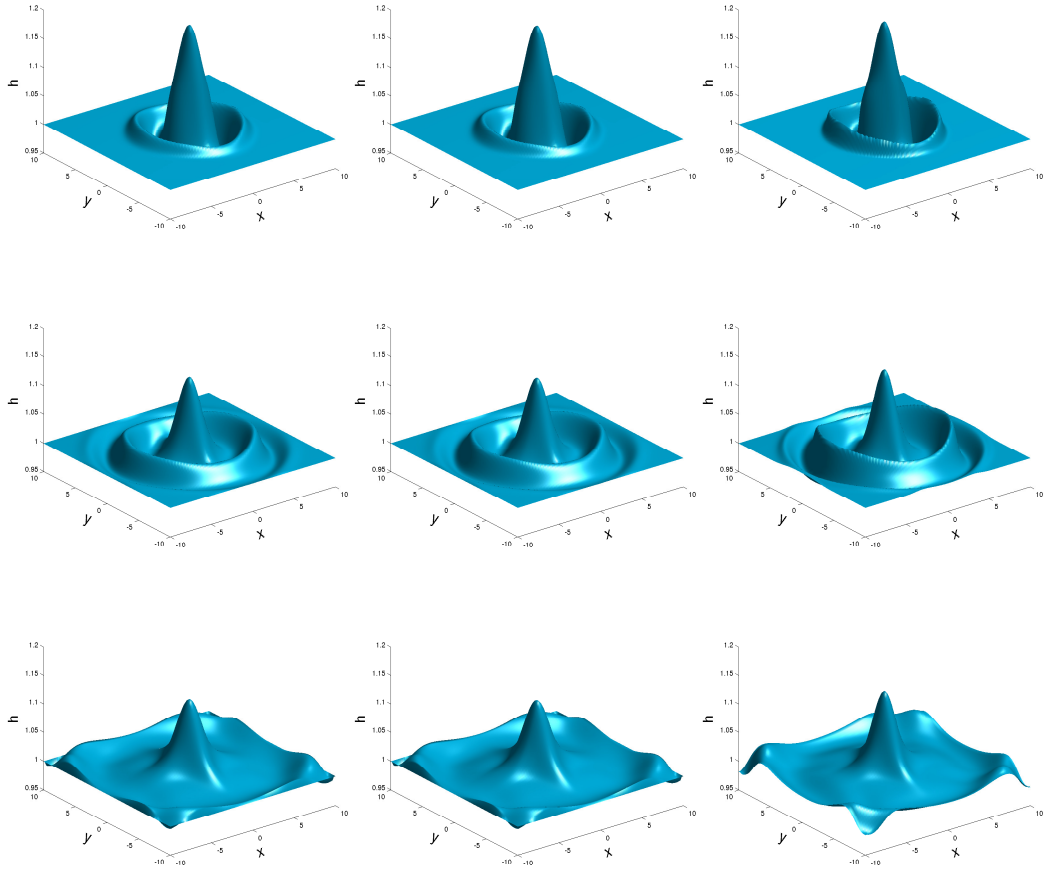

Fig. 6. Water depth for the circular dam-break problem on flat bottom obtained at different times using Roe (first column), SRNH (second column) and FVC (third column). From top to bottom $t = 4$, 8 and 16.

4.2 Circular dam-break problem

This example was proposed in [8] to study cyclone/anticyclone asymmetry in nonlinear geostrophic adjustment. We solve the shallow water equations (1) on a flat bottom in the spatial domain $\Omega = [-10, 10] \times [-10, 10]$ subject to Neumann boundary conditions and equipped with the following initial conditions

$$h(0, x, y) = 1 + \frac{1}{4}\left(1 - \tanh\left(\frac{\sqrt{ax^2 + by^2} - 1}{c}\right)\right), \quad u(0, x, y) = v(0, x, y) = 0,$$

where $a = \frac{5}{2}$, $b = \frac{2}{5}$ and $c = 0.1$. In our simulations $g = 1$ and $f_c = 1$ as in [8] and two meshes of 50×50 and 100×100 gridpoints are considered. In Figure 5 we illustrate the initial conditions used for this test example. The plots of the computed water height are shown in Figure 6 at three different times $t = 4$, 8 and 16 using a mesh of 100×100 gridpoints. In this figure we have

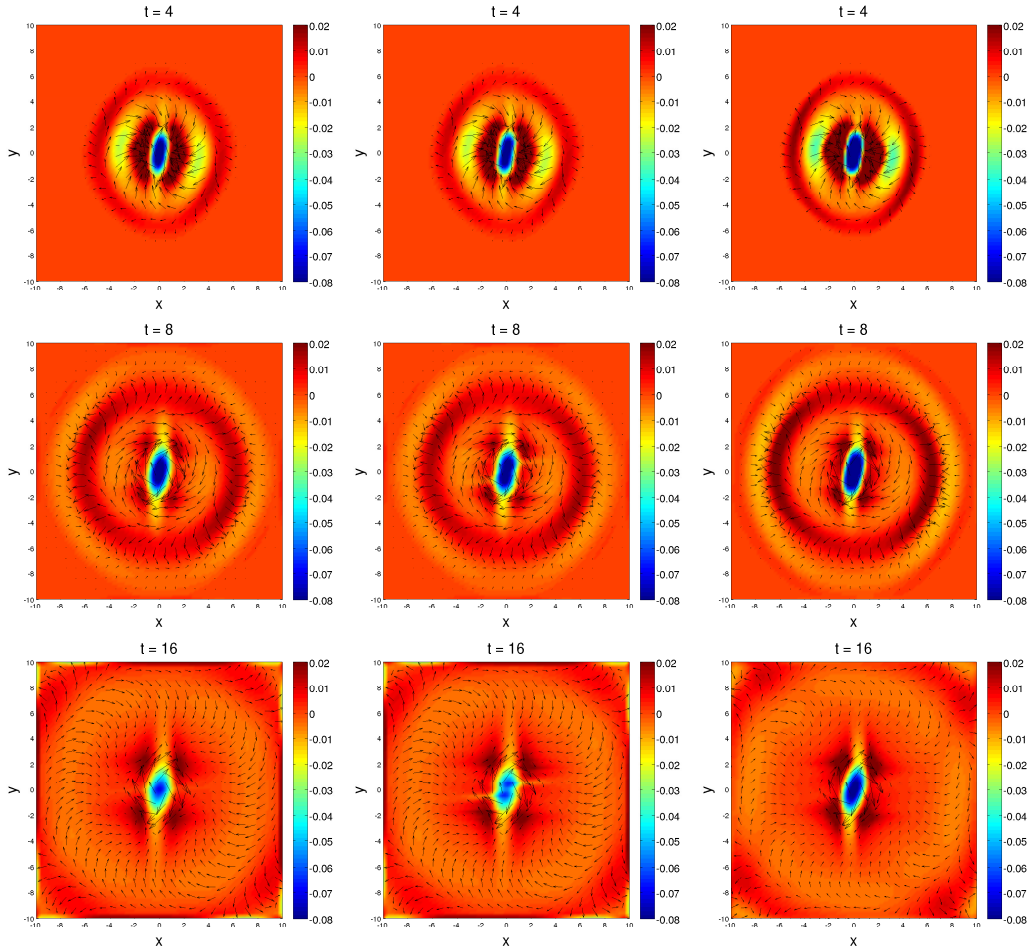

Fig. 7. Vorticity plots and velocity fields for the circular dam-break problem on flat bottom obtained at different times using Roe (first column), SRNH (second column) and FVC (third column). From top to bottom $t = 4$, 8 and 16.

also included the results obtained using the Roe and SRNH for comparison. As can be seen a bore has formed and the water drains from the deepest region as a rarefaction wave progresses outwards. It is clear from the presented results that the initial elliptical mass imbalance evolves in a nonaxisymmetric way. The two expected shock waves are very well captured by the proposed FVC method. These results are qualitatively in good agreement with those published in [8].

In Figure 7 we exhibit the results for the vorticity variable and the velocity field obtained using the considered methods. As can be seen the two shock waves originated behind the water elevation are slowly spinning clockwise in the computational domain. The velocity field is well represented by the FVC method and recirculation regions within the flow domain are well captured. For the considered simulation times, numerical results obtained using FVC method appear to be more accurate than those obtained using Roe and SRNH methods. For instance, the numerical diffusion is very pronounced in Roe and

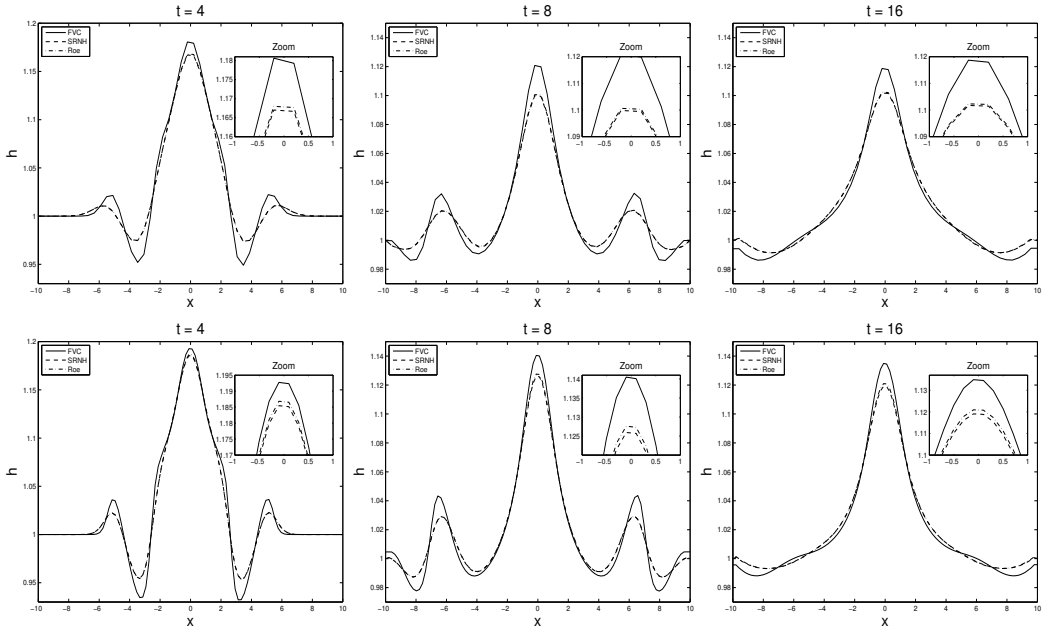

Fig. 8. Diagonal cross-sections of the water depth at $y = x$ for the circular dam-break problem on flat bottom obtained at different times using 50×50 gridpoints (first row) and 100×100 gridpoints (second row).

SRNH schemes applied to this flow problem on the mesh with 100×100 gridpoints. Furthermore, the numerical diffusion is more pronounced in the results obtained using Roe and SRNH schemes than the FVC method. To further illustrate this effect we present in Figure 8 diagonal cross-sections of the water depth at $y = x$ for two meshes with 50×50 and 100×100 gridpoints. It is clear that on the coarse mesh with 50×50 gridpoints the numerical diffusion in the results obtained using Roe and SRNH schemes is larger than the FVC method. Refining the mesh to 100×100 gridpoints the numerical diffusion in Roe and SRNH schemes reduces but the results obtained using FVC method are the most accurate. It is worth mentioning that for this test problem, the computational time required for the FVC method is about 5 times less than for Roe and SRNH schemes. This is a huge saving in the computational cost as the proposed FVC method is faster and more accurate than the Roe method widely used in the literature to solve this class of applications in shallow water flows.

Our next concern is to assess the performance of our FVC method to solve this circular dam-break problem on a non-flat bottom. Hence, we solve the same test problem on a non-flat bed defined as

$$Z(x, y) = 0.3 \left(1 + \tanh\left(\frac{3x}{2}\right)\right).$$

The computed results for the water depth obtained at $t = 2$, 8 and 16 using two meshes with 100×100 and 200×200 gridpoints are displayed in Figure 9.

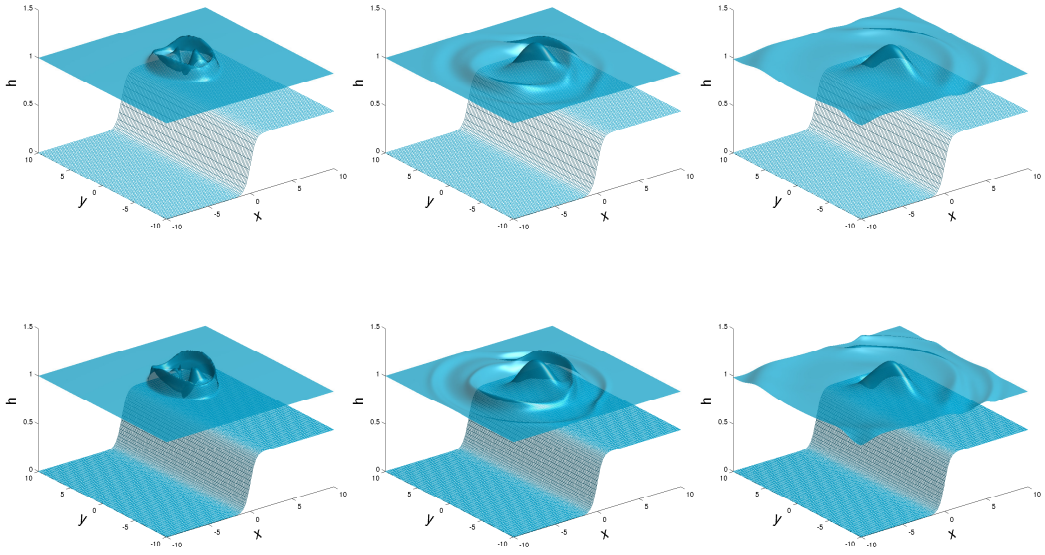

Fig. 9. Water depth for the circular dam-break problem on non-flat bottom obtained using a mesh with 100×100 gridpoints (first row) and 200×200 gridpoints (second row). From left to right $t = 2$, 8 and 16.

The corresponding results for vorticity variable and velocity field are presented in Figure 10. From a numerical point of view this test example is more difficult than the previous one as the flow is expected to exhibit complex features due to the interaction between the water surface and the bed. As in the previous test a bore has formed and the water drains from the deepest region as a rarefaction wave progresses outwards. However, a slower propagation is detected for the water free-surface in this test compared to the previous one and larger values of the vorticity are also observed for this example compared to the simulations on flat-bottom. The FVC method resolves accurately the flow structures and the vortices seem to be localized in the correct place in the flow domain. In addition, the resolution of the FVC method is clearly observed and no oscillations have been detected in the vicinity of the bed transition.

As for the previous test example, in Figure 11 we compare the results obtained using FVC scheme to those obtained using Roe and SRNH methods. Here we present diagonal cross-sections of the water depth at $y = x$ on the mesh with 50×50 gridpoints at different times. For a better insight zooming plots have been included within the results. Numerical results obtained using the FVC scheme appear to be more accurate than those obtained using Roe and SRNH methods, observe the differences at the hydraulic jump at times $t = 8$ s and $t = 16$ s. A comparison of CPU times is also carried out for this problem and it is summarized in Table 2. It is clear that the FVC scheme is more efficient than the Roe and SRNH methods. For instance, at time $t = 16$ s the CPU time for Roe and SRNH schemes is about 12 times more than the FVC

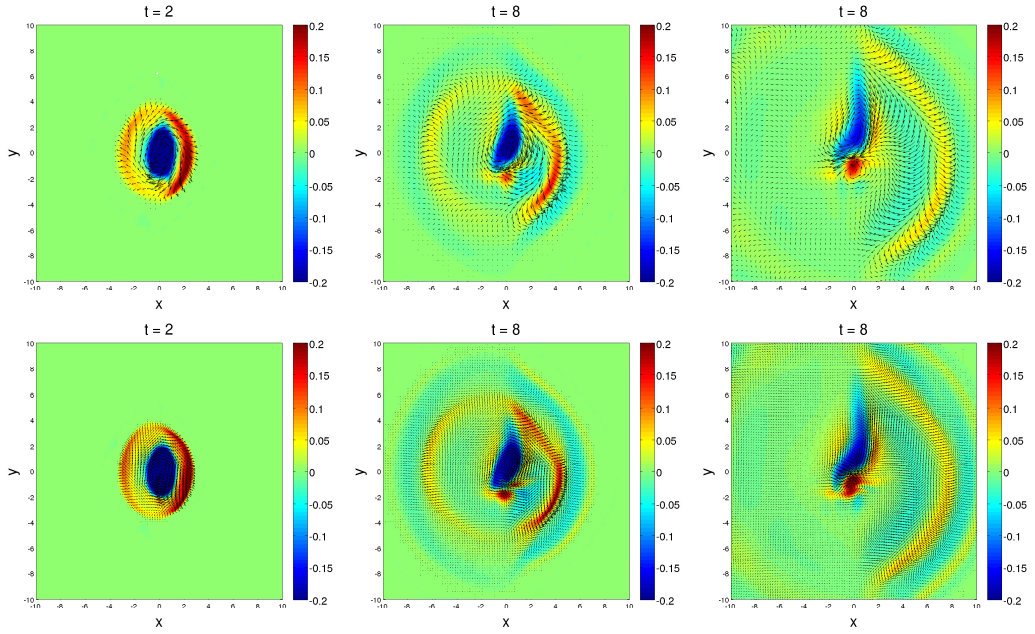

Fig. 10. Vorticity plots and velocity fields for the circular dam-break problem on non-flat bottom obtained using a mesh with 100×100 gridpoints (first row) and 200×200 gridpoints (second row). From left to right $t = 2$, 8 and 16.

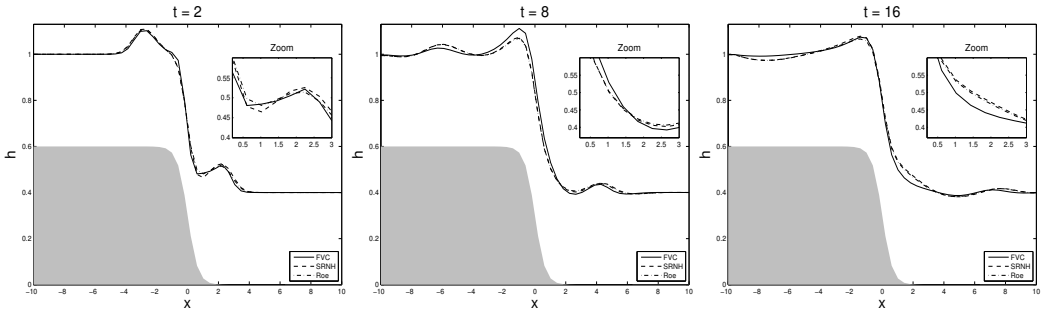

Fig. 11. Diagonal cross-sections of the water depth at $y = x$ for the circular dam-break problem on non-flat bottom obtained at different times using a mesh with 50×50 gridpoints.

scheme. Balancing the accuracy reported in Figure 11 and the computational cost in Table 2, the FVC scheme can be considered as a highly efficient solver for this type of shallow water flows over non-flat beds.

4.3 Periodic shear-layer flow

Our final test example consists of the periodic shear-layer problem solved in [9] using the Navier-Stokes equations. In the current study we consider the case with zero viscosity which is most challenging to numerically solve. Similar periodic shear-layer problems have also been studied in [3] among others. The

Table 2
CPU times (in seconds) obtained for the circular dam-break problem on non-flat bottom obtained at different times using a mesh with 50×50 gridpoints.

	$t = 2\ s$	$t = 8\ s$	$t = 16\ s$
Roe	2.18	8.10	16.44
SRNH	2.38	8.27	16.57
FVC	0.28	0.78	1.41

computational domain $\Omega = [-\frac{1}{2}, \frac{1}{2}] \times [-\frac{1}{2}, \frac{1}{2}]$ and the initial conditions are $h(0, x, y) = 1$,

$$u(0,x,y) = \begin{cases} -\dfrac{1}{2}, & (x,y) \in [-\dfrac{1}{2}, \dfrac{1}{2}] \times [-\dfrac{1}{20}, \dfrac{1}{20}], \\ \dfrac{1}{2}, & \text{elsewhere,} \end{cases}$$

and

$$v(0,x,y) = \begin{cases} \dfrac{1}{10} \sin(4\pi x), & (x,y) \in [-\dfrac{1}{2}, \dfrac{1}{2}] \times [-\dfrac{1}{20}, \dfrac{1}{20}], \\ 0, & \text{elsewhere.} \end{cases}$$

Periodic boundary conditions are used and the remaining parameters are $g = 1$ and $f_c = 0.01$. The objective of this test problem is to check the performance and stability of the proposed FVC method to resolve the small perturbations on the water free-surface and vorticity in the rotating and mixing shallow water flows. We use a mesh with 100×100 gridpoints in our simulations.

Figure 12 presents the obtained results for water depth, vorticity and velocity field at times $t = 1$, 2 and 4. From a simple inspection on this figure we can see, the two small regions of the circulation occurring in the center of the computational domain, the predicted vortices with increased water depth near the upper and lower bands, and the predicted velocity distribution that causes the water surface to recirculate. It can be easily seen that the small complex structures of the water flow being captured by our FVC method. There is excellent agreement between these results and those published in [9] using a different approach based on the well-known Navier-Stokes equations.

It should be stressed that the proposed FVC method is a modular algorithm into which any high-order interpolation procedure and any high-order time stepping scheme can easily be incorporated. Note that the method presented in this paper can be highly optimized for the vector computers, because they not require nonlinear solvers and contain no recursive elements.

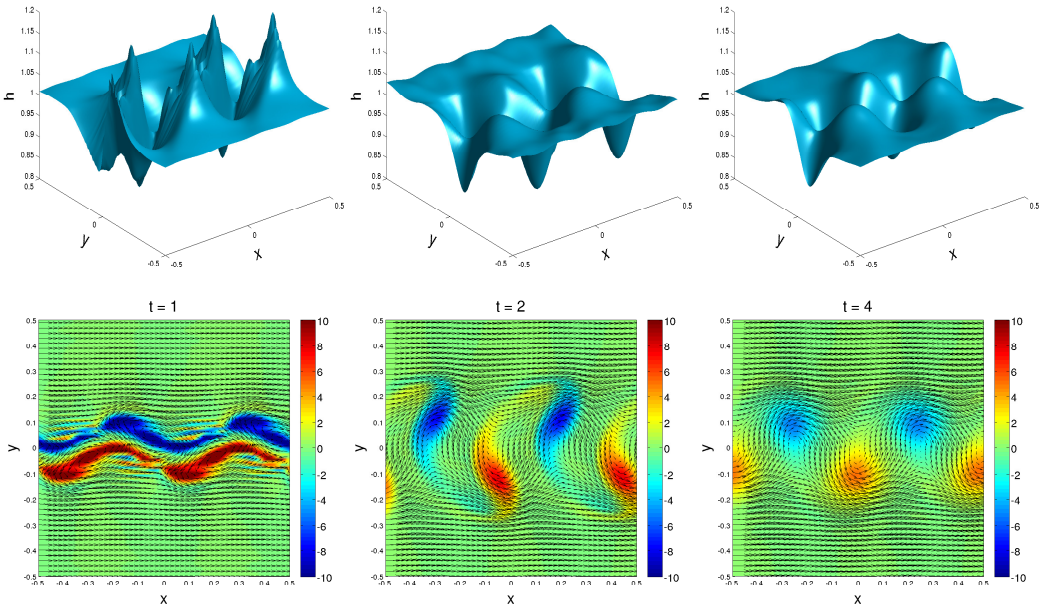

Fig. 12. Water depth (first row), vorticity plots and velocity fields (second row) for the periodic shear-layer problem obtained using a mesh with 100×100 gridpoints. From left to right $t = 1$, 2 and 4.

5 Conclusions

We have presented a fast and accurate projection finite volume characteristics method to solve two-dimensional shallow water equations on both flat and non-flat beds. The proposed method uses advantages of the method of characteristics in a finite volume discretization of the shallow water system. In terms of advantages, the method can solve steady flows over irregular beds without large numerical errors, thus demonstrating that the proposed scheme achieves perfect numerical balance of the gradient fluxes and the source terms. In addition, the method can compute the numerical flux corresponding to the real state of water flow without relying on Riemann problem solvers. Reasonable accuracy can also be obtained easily and no special treatment is needed to maintain a numerical balance, because it is performed automatically in the integrated numerical flux function. In addition, the proposed approach does not require either nonlinear solution of algebraic equations or special front tracking techniques. Furthermore, it has strong applicability to various problems in rotating shallow water flows as shown in the presented numerical results.

The proposed finite volume characteristics method has been tested on systems of shallow water equations at different flow regimes. The method has also been compared to other well-established finite volume methods for shallow water equations. The obtained results indicate good shock resolution with high ac-

curacy in smooth regions and without any nonphysical oscillations near the shock areas. The well-balancing property of the method has been verified in flow at rest on non-flat bottom. Although we have restricted our numerical computations to structured meshes, the current finite volume characteristics scheme can be extended to rotating shallow water flows in two space dimensions with bottom friction using unstructured grids. These and further issues are subject of future investigations.

References

[1] F. Alcrudo, F. Benkhaldoun, Exact solutions to the Riemann problem of the shallow water equations with a bottom step, Computers & Fluids. 30 (2001) 643-671.

[2] E. Audusse, R. Klein, A. Owinoh, Conservative discretization of Coriolis force in a finite volume framework, J. Comp. Phys. 228 (2009) 2934-2950.

[3] J.B. Bell, P. Colella, H.M. Glaz, A second-order projection method for the incompressible Navier-Stokes equations, J. Comp. Phys. 85 (1989) 257-283.

[4] F. Benkhaldoun, M. Seaid, A simple finite volume method for the shallow water equations, J. Comp. Applied Math., 234 (2010) 58-72.

[5] F. Benkhaldoun, I. Elmahi, M. Seaid, A new finite volume method for flux-gradient and source-term balancing in shallow water equations, Comput. Meth. in Appl. Mech. Eng. 199 (2010) 49-52.

[6] A. Bermudez, M.E. Vázquez-Cendón, Upwind methods for hyperbolic conservation laws with source terms, Computers & Fluids. 23 (1994) 1049-1071.

[7] U.S. Fjordholm, S. Mishra, Vorticity preserving finite volume schemes for the shallow water equations, SIAM J. Sci. Comput 33 (2011) 588-611.

[8] A.C. Kuo, L.M. Polvani, Nonlinear geostrophic adjustment, cyclone/anticyclone asymmetry, and potential vorticiy rearrangement, Phys. Fluids. 12 (2000) 1087-1100.

[9] C.D. Munz, L. Schmidt, Numerical simulation of compressible hydrodynamic instabilities with high resolution schemes, In Nonlinear Hyperbolic Equations, Notes on Numerical Fluid Dynamics 24 (1988) 456-465.

[10] A. Robert, A stable numerical integration scheme for the primitive meteorological equations, Atmos. Ocean 19 (1981) 35-46.

[11] P.L. Roe, Approximate Riemann solvers, parameter vectors and difference schemes, J. Comp. Phys. 43 (1981) 357-372.

[12] S. Sahmim, F. Benkhaldoun, F. Alcrudo, A sign matrix based scheme for quasi-hyperbolic non-homogeneous PDEs with an analysis of the convergence stagnation problem, J. Comp. Phys. 226 (2007) 1753-1783.

[13] M. Seaid, Non-oscillatory relaxation methods for the shallow water equations in one and two space dimensions, Int. J. Numer. Methods Fluids. 46 (2004) 457-484.

[14] M. Seaid, On the quasi-monotone modified method of characteristics for transport-diffusion problems with reactive sources, Comp. Methods App. Math. 2 (2002) 186-210.

[15] S. Vukovic, L. Sopta, ENO and WENO schemes with the exact conservation property for one-dimensional shallow-water equations, J. Comp. Phys. 179 (2002) 593-621.

[16] Y. Xing, C. Shu, High order well-balanced finite volume WENO schemes and discontinuous Galerkin methods for a class of hyperbolic systems with source terms, J. Comp. Phys. 214 (2006) 567-598.